

東京大学 大学院新領域創成科学研究科
基盤科学研究系
先端エネルギー工学専攻

平成 18 年度

修士論文

Position control of a superconducting magnet-floating coil
in a magnet-sphere-shaped plasma device RT-1

磁気圏型プラズマ装置 RT-1 における
超伝導磁気浮上コイルの位置制御

2007 年 2 月提出
指導教員 吉田 善章 教授

56220 矢野善久

Contents

Contents	2
List of Figures	5
List of Tables	6
1 Introduction	8
2 RT-1 Device	10
3 z-axis Instability	17
3.1 Basic equations	17
3.2 Linear analysis	19
3.3 Nonlinear analysis	20
3.3.1 Mutual inductance between F-coil and L-coil	21
3.3.2 z dependence of I_F and I_L	22
3.3.3 z-axis instability in the nonlinear analysis	23
3.4 Consideration	23
4 Levitation Control System of RT-1	26
4.1 Model of Levitation Control System of RT-1	28
4.1.1 Laser position detector	28
4.1.2 PID controller	31
4.1.3 L-coil current and an effect of the eddy current	34
4.1.4 z-axis motion of F-coil	37
4.1.5 Block-diagram of RT-1 levitation system	38
4.2 Mock-up experiment	40
4.2.1 Levitation experiment of RT-1 F-coil	44
5 Correction Experiment of Error Field and Mass Imbalance	47
5.1 Mechanism of tilting and rotation	49

5.2	Error field and mass imbalance	52
5.3	Experimental setup	54
5.4	Experimental result	58
5.4.1	Accelaration of F-coil rotation motion	58
5.4.2	$\phi - \theta$ plots	60
5.4.3	Correction of error field	62
5.4.4	Correction of mass imbalance	63
6	Summary	66
	Acknowledgments	67
	Bibliography	68
	Publications	69

List of Figures

2.1	Photographic view of the RT-1	10
2.2	Schematic view of RT-1 Device	11
2.3	Magnetic field of Rt-1 floating coil and levitation coil	13
2.4	The scematic veiw of the relations of F-coil and L-coil and PD positions.	14
2.5	Schematic view of the RT-1 center stack structure. The elevator brings up and down the floating coil between the levitation region and maintenance chamber. The coil catcher can open within 0.1s before the floating coil falls down 5cm.	15
2.6	Photographic view of F-coil catcher. The cathcer is opened in this photograph.	16
3.1	The sketch of the model of force balance to the z direction.	18
3.2	z-dependence of z-axis instability by linear analysis	19
3.3	Calculation results of z-dependence (upper) and z-differential (lower) of mutual inductance	21
3.4	Clculation results of z dependence of I_{L+} (red line) and I_{F+} (blue line)	24
3.5	Calculation results of z dependence of I_{L-} (red line) and I_{F-} (blue line)	24
3.6	Calculation results of z dependence of α_+ (upper) and α_- (lower)	25
4.1	Flowchart of levitation controll system of RT-1 HTS coil. Position Detector's signal is negative-feedbacked to PIDcontroller.	27
4.2	The schematic view of the Lasor position Ditector arrangement.	29
4.3	F-coil z-position dependence of LPD output voltage.	30
4.4	Main circuite of RT-1 PID controller.	32
4.5	Gain plots of the P,I,D each element and whole PID.	33
4.6	The schematic view of the experiment.	35
4.7	The schematic view of measurement of frequency responce. Gain is nora- malized by f=1. Lines are fitting line which fitted as first order lag element.	36
4.8	Block diagram of RT-1 system.	38

4.9 Pole configuration of RT-1 system. Unstable pole moved to stable area by PID feedback control.	39
4.10 Nyquist diagram of RT-1 feedback control systme.	39
4.11 Main circuite of mock-up circuite.	41
4.12 Block diagram of this experiment. Mock-up circuite is substituted for F-coil.	42
4.13 Stepresponse of hall sensor output voltage. Hall sensor output is normalized.	43
4.14 Stepresponse of z position.	44
4.15 Frequency response of RT-1 F-coil system.	45
4.16 Comparison of the stepresponse between an actual F-coil response and a calculation result of the model.	45
4.17 Margin of the gain g_M and the phase delay ϕ_M which is calculated by nyquist diagram.	46
5.1 Tilting and pendulum and oscilating motions.	48
5.2 Schematic drawing of tiling.	49
5.3 Schematic drawing of tilting. (2)	49
5.4 Schematic drawing of tilting. (3)	50
5.5 Schematic drawing of pendulum motion of the coil.	51
5.6 Schematic view of the model.	53
5.7 Calculation result of the model. Broken lines are sine fitting lines of the same color.	53
5.8 Transform coefficient k_B and k_M	55
5.9 Schematic view of correction coils.	56
5.10 Photographic view of correction coils. Blue cords are collection coils.	57
5.11 Signal of pendulum motion. It is easily to see θ bounds. In this shot, $I_{NS}=7.05A$ $I_{EW}=4.07A$ and z position is 27mm.	58
5.12 Signal of fast rotation motion. θ does not bound. In this shot, $I_{NS}=7.05A$ $I_{EW}=4.55A$ and z position is 27mm.	59
5.13 $\phi - \theta$ plots of 5.11. Red line is actual plots and blue broken line is sine fitting curve. Because of pendulum motion, red line is not closed.	60
5.14 $\phi - \theta$ plots of 5.12. Red line is actual plots and blue broken line is sine fitting curve. Because of fast rotation motion, red line is closed.	61
5.15 Correction current dependence of ϕ_{NS} and ϕ_{EW} . Experiment was carried out by 3terms. Line color represents the same term. These shots are measured at z position = 0mm	62
5.16 Balance configuration before correction of mass imbalance.	63
5.17 Balance configuration after putting a weight on.	64

5.18 Balance configuration after moving built-in balancers.	64
5.19 Final balancer configuration	65
5.20 Levitation signal.	65

List of Tables

2.1	Principal parameter of RT-1	12
-----	---------------------------------------	----

Chapter 1

Introduction

RT-1 device is constructed to verify the role of the plasma flow in confinement. Mahajan-Yoshida[1, 2] has studied about a plasma relaxation under the condition of strong plasma flow as fast as Alfvén velocity. And this relaxation state has a possibility to confine a high β plasma observed at magnetosphere of Jupiter[3] and it is expected to achieve a advanced nuclear fusion.

The concept of RT-1 is a dipole shaped magnetic field like magnetosphere of planet. To generate dipole field, RT-1 device has a high temperature superconducting (HTS) internal coil. Because HTS coil has laege current density and permanent current , RT-1 HTS coil can not only generate a strong dipole field but also float above the support in the vacuum chamber long time. When there're no object such as supports or rods inside of the separatrix, "detouchment" plasma parameter is expected to be much proved . Now in the levitation experiment, we levitate the HTS coil about 10mm-30mm above the support from the point of view of coil protection. To achieve the detouchment plasma, we should study a property of levitation control system and HTS coil motion.

In the RT-1, HTS coil is levitated by normal conducting levitation coil which is installed above the RT-1 vacuum chamber. This type of levitation is always unstable to the z -axis (garavity direction) motion , always stable to the (x, y) -axis motion and, under certain circumstances stable to (θ_x, θ_y) axis motion.

Instability of z -axis motion can be analyzed by the motion equation of HTS coil linearly. And by including a conservation law of magnetic flux, which is a special feature of superconducting coil, a nonlinear analysis is possible. The effect of an conservation law of magnetic flux has always stability effect, but in RT-1 device an effect of a conservation law of magnetic flux is much less than it's linear instability.

In RT-1, instability of a z -axis motion is stabilized by the levitation coil current which is PID feedback controled. RT-1 levitation system consists of the HTS floating coil, the levitaion power supply, the levitation coil, the PID feedback controller and 3 pieces of

laser position detector. Because the levitation coil is set up on the outside of the chamber, effect of an eddy current of the chamber is measured. By using an approximation model of HTS coil motion, a block diagram of the RT-1 levitation feed back control system can be determined. This research also measured a stepresponse of RT-1 levitation feedback control system.

One more subject around the levitation was discovered that HTS coil's attitude is tilting about 2 degs and the coil rotates slowly from side to side like a pendulum. Tilt may degrade a precision of magnetic field and lead a lack of axisymmetry of plasma. And the coil intermittently oscillates during rotation. Because the coil motion is described by a balance between electromagnetic force and gravity force, an error magnetic field around the coil and the coil's mass unbalance are causes of a tilt. This tilting attitude and the "pendulum" motion is closely related, because the tilting attitude generates newly a rotation force on the coil.

In this research, we aim to construct a plasma device of 10^{-3} magnetic field accuracy. We made an experiment on canceling an errorfield by two pair of "correction coils" . And we also made an experiment on correcting a mass balance by putting balancers or weights on the coil's case to reduce a mass imbalance to less than 0.057deg which is needed to achieve 10^{-3} accuracy.

Chapter 2

RT-1 Device

The Ring Trap 1 (RT-1) device shown in figure.2.1 and 2.2 is aiming to explore a fast flow plasma physics. This device can generate a magnetosphere-like magnetic field by a high temperature superconducting (HTS) coil levitated in the vacuum chamber. The

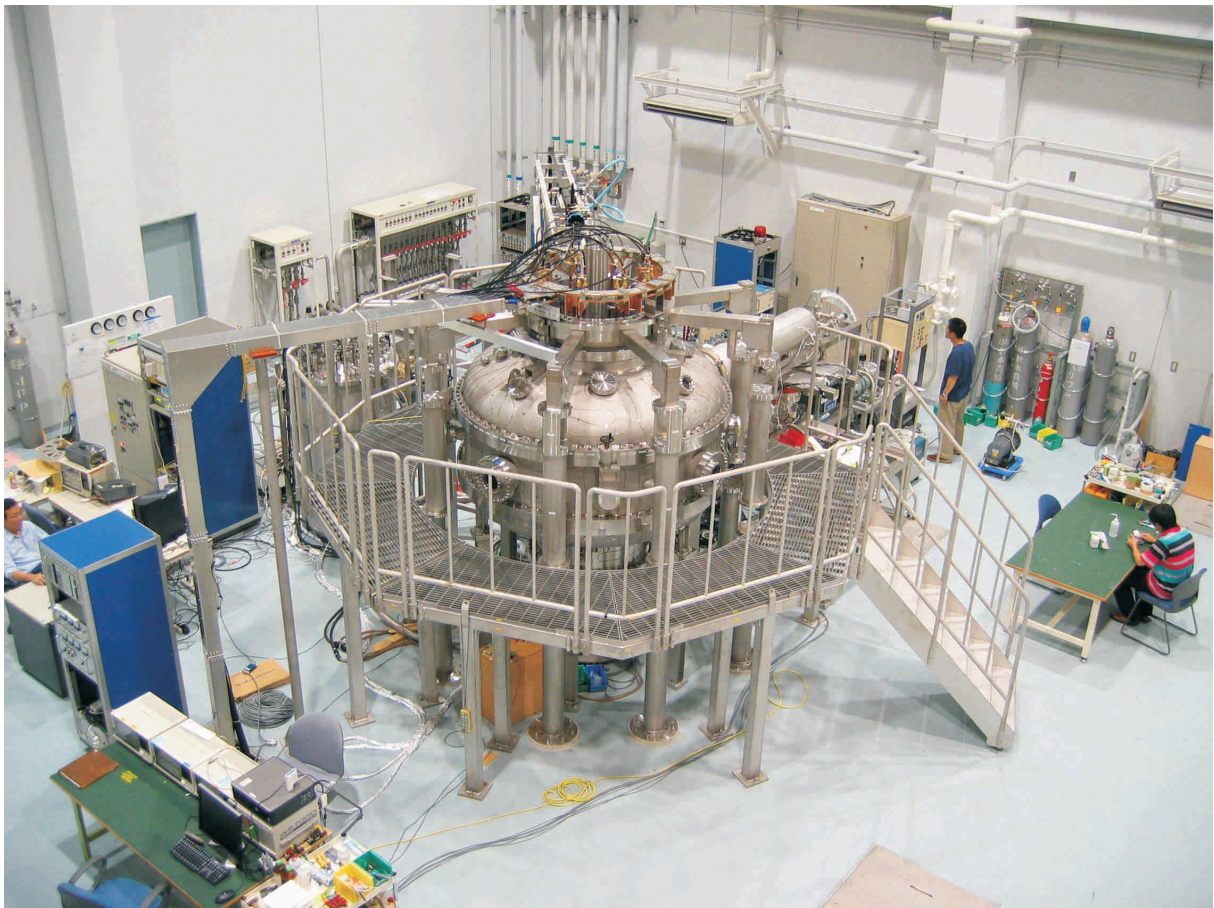


Figure 2.1: Photographic view of the RT-1

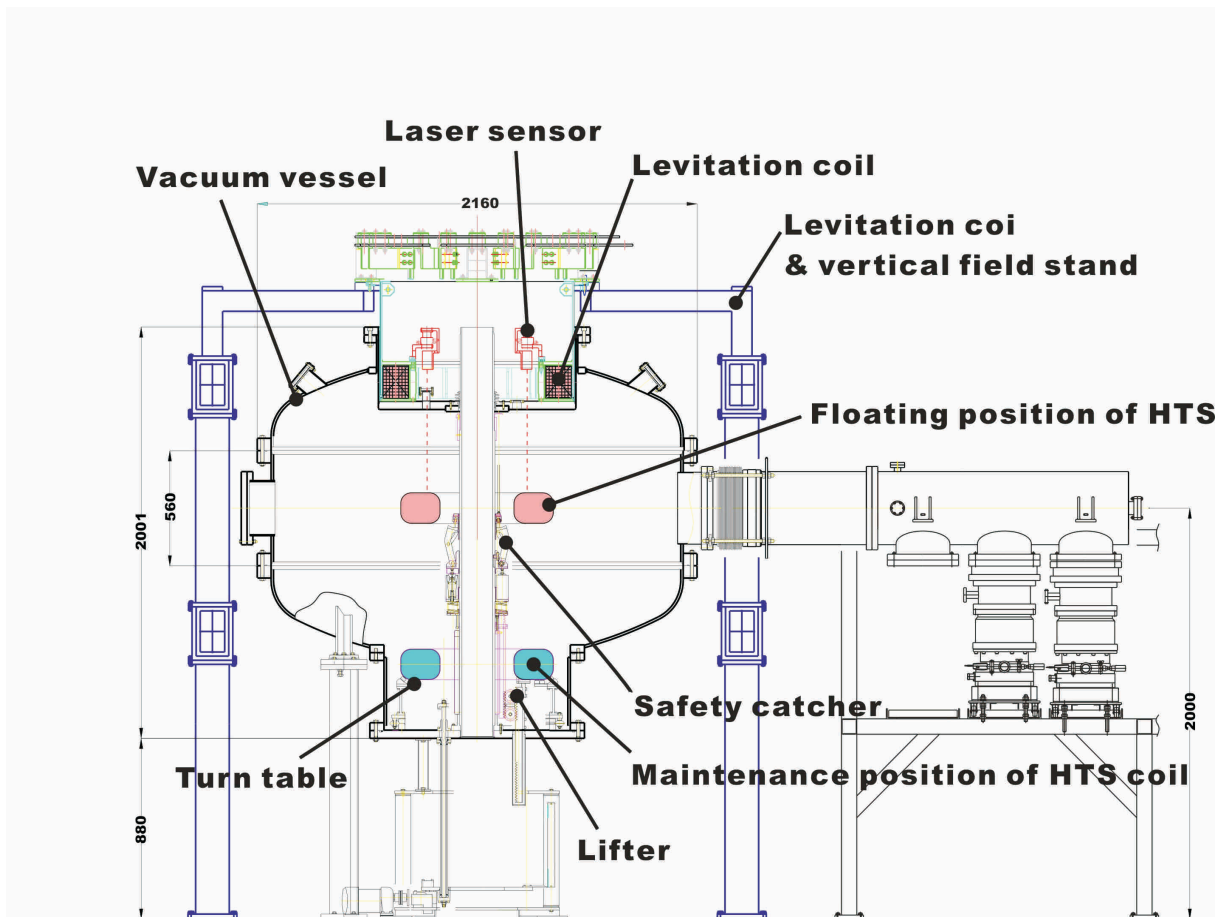


Figure 2.2: Schematic view of a dipole plasma confinement device RT-1. This device is able to generate a plasma with the superconducting internal conductor levitated by levitation coil.

HTS coil is levitated by a normal conducting levitation coil which is set up at the top of the vacuum chamber. A maintenance space is at the bottom of the chamber, where the HTS coil is cooled and charged.

The HTS coil is made of Bi-2223 high temperature superconductor, and it weighs about 112kilograms. The HTS coil is charged to 116A per 1 turn and the coil has a total of 2160 turns so the coil has 250kA as a total current. The magnetic field strength in the confinement region varies from 0.3T to 0.03T. An outside radius of the coil is 0.375m and an inside radius is 0.18m and a radius of a current center is 0.25m. The HTS coil has a permanent current switch, which can switch on the permanent current mode. The HTS coil has many other functions in the coil case, which relate to the operation of cooling and charging and monitoring.

The levitation coil is made of copper. The coil has a total of 68turns and the coil

Table 2.1: Principal parameter of RT-1

Vacuum vessel	Inner radius	1000mm
	Height	560m
HTS ring coil	Major radius	250mm
	Outside radius	375mm
	Inside radius	180mm
	Height	150mm
	Coil wire	2160 turns (Bi-2223)
	Excitation current	116A
	Magnetic field strength	0.03 - 0.3T
	Mass	112kg
	Operation temperature	20-30K
	Self inductance	3.3H
	Stored energy	22kJ
Levitation coil	Major radius	400mm
	Coil wire	68 turns (copper)
	DC power supply	1500A DC / 150A AC
	Magnetic field strength	0.003-0.03T
	Resistance	28m Ω
	Self inductance	4.6mH
RF heating1	Frequency	8.2GHz
	Power	100kW
	Pulse width	1sec
RF heating2	Frequency	2.5GHz
	Power	20kW
	Pulse width	2sec
Coil catcher	Response speed	0.1s

current is about 440A per 1turn in the usual levitating operation so the coil has a total 30kA current. A radius of a current center is 0.40m. A rated current of a power supply of the coil is 1500A DC and 150A AC. In the usual levitation condition, the magnetic field of levitation coil is about 0.01T near the HTS coil and 0.003 – 0.03T in the plasma confinement region. The levitation coil is located at $z=612\text{mm}$ (figure.2.4).

The magnetic field made by RT-1 floating coil and levitation coil is shown in figure.2.3 . The outer most magnetic surface is expressed by a green bold line.

F-coil is stabilized by L-coil current by PID feedback controll. In the RT-1 device, z position of F-coil is measured by 3-cord of lasor position detectors (LPD). Position

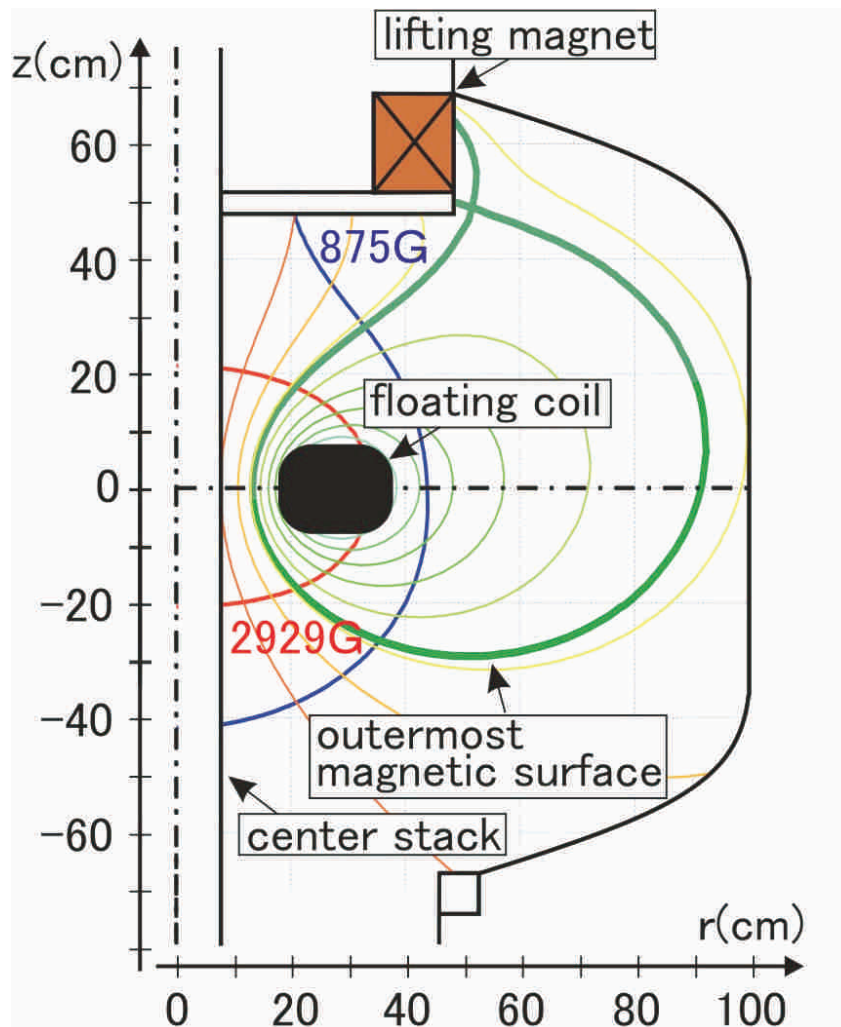


Figure 2.3: Magnetic field of Rt-1 floating coil and levitation coil

detectors are located at $z=600\text{mm}$ on every 120deg s. The schematic view of the relations of F-coil and L-coil and PD positions is shown in figure.2.4. This figure also shows the cross sections of the F-coil and L-coil.

The maintenance chamber is located at the bottom of RT-1 chamber and the coil support stage moves up to the levitation region and down to the maintenance chamber. In the maintenance chamber, there are two coolant transfer tubes and two current leads and three monitoring connectors. First, the HTS coil is cooled to 20K here and charged to 250kA then lifted up to the levitation region to experiment. We can continue the superconducting operation for about 7 hours before the coil temperature increases to 30K . The current decay is less than 1. After the experiment, the coil is lifted down to the maintenance space to cool the coil again or to rise the coil temperature. The schematic view of the RT-1 maintenance chamber and elevator is shown in figure.2.5.

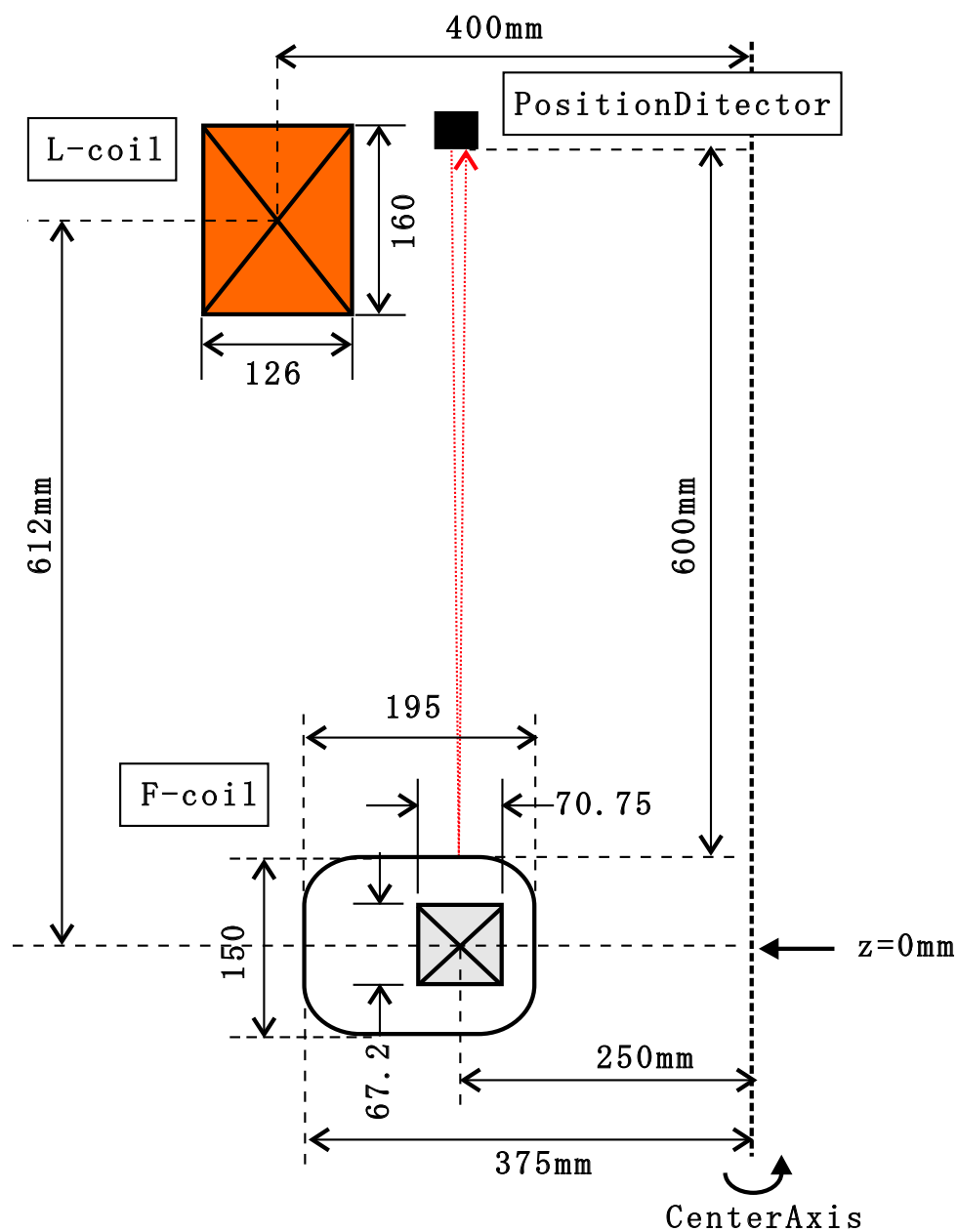


Figure 2.4: The schematic view of the relations of F-coil and L-coil and PD positions.

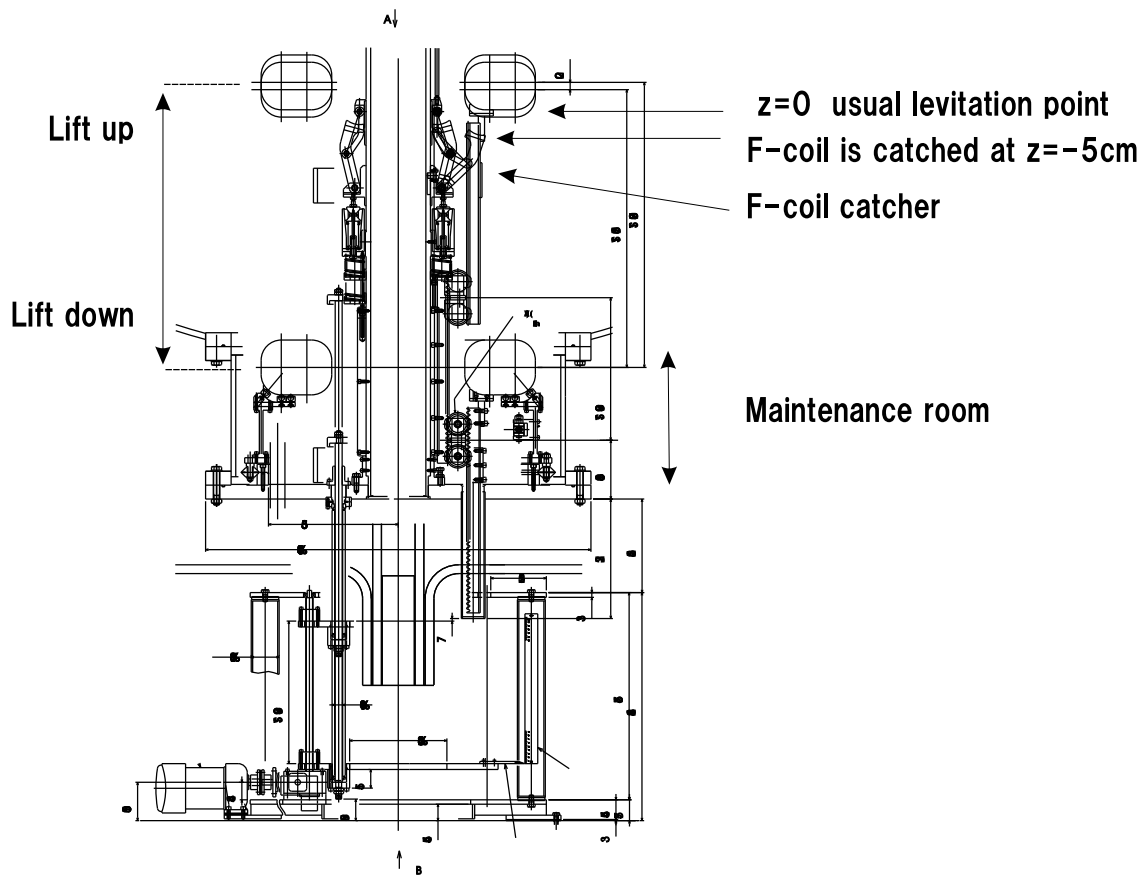


Figure 2.5: Schematic view of the RT-1 center stack structure. The elevator brings up and down the floating coil between the levitation region and maintenance chamber. The coil catcher can open within 0.1s before the floating coil falls down 5cm.

RT-1 device can produce plasma by 1sec. pulse 8.2GHz (MAX 100kW power) microwave and 2sec.pulse 2.5GHz (MAX 20kW power) microwave.

There's also the coil's catcher which can catch the coil in case of accidental drop such as an earthquake or a power failure. The catcher is set up on the center stack of the RT-1 chamber. When the accidental signal comes to the catcher, the catcher can open within 0.1sec while the coil falls down about 5cm. The photographic view of the catcher is shown in figure.2.6.



Figure 2.6: Photographic view of F-coil catcher. The catcher is opened in this photograph.

Chapter 3

z-axis Instability

This chapter we obtain a z-axis instability of RT-1 HTS coil (F-coil). When defining whether some rigid body is stable or not here, we judge whether there is any righting moment when there's a gap from some steady state. And we define α for a quantity of instability here. α means growth rate of motion, and $\alpha > 0$ means unstable.

First we analyze a z-axis instability linearly by using an equation of the coil motion. Next we go forward to nonlinear analysis by including the equation of flux conservation of F-coil.

3.1 Basic equations

The motion equation of F-coil to z-direction is written as

$$m \frac{d^2 z}{dt^2} = 2\pi R \cdot I_F \cdot B_r - mg \quad (3.1)$$

where m is F-coil mass, z is z position of the coil, R is major radius of the F-coil current, I_F is F-coil current, B_r is the magnetic field the F-coil feels to the radial direction, g is the gravitational acceleration. And also the equation of flux conservation of F-coil is written as

$$\frac{d}{dt}(L_F \cdot I_F + M \cdot I_L) = 0 \quad (3.2)$$

where L_F is an inductance of F-coil, M is a mutual inductance between the levitation coil (L-coil) and F-coil, I_L is L-coil current.

We must note that B_r is a function of (I_L, z) and M is a function of (z) , I_F is a I_L function. Then we easily see that these two simultaneous equations are complicatedly coupling.

The schematic view of this model is shown in figure.3.1.

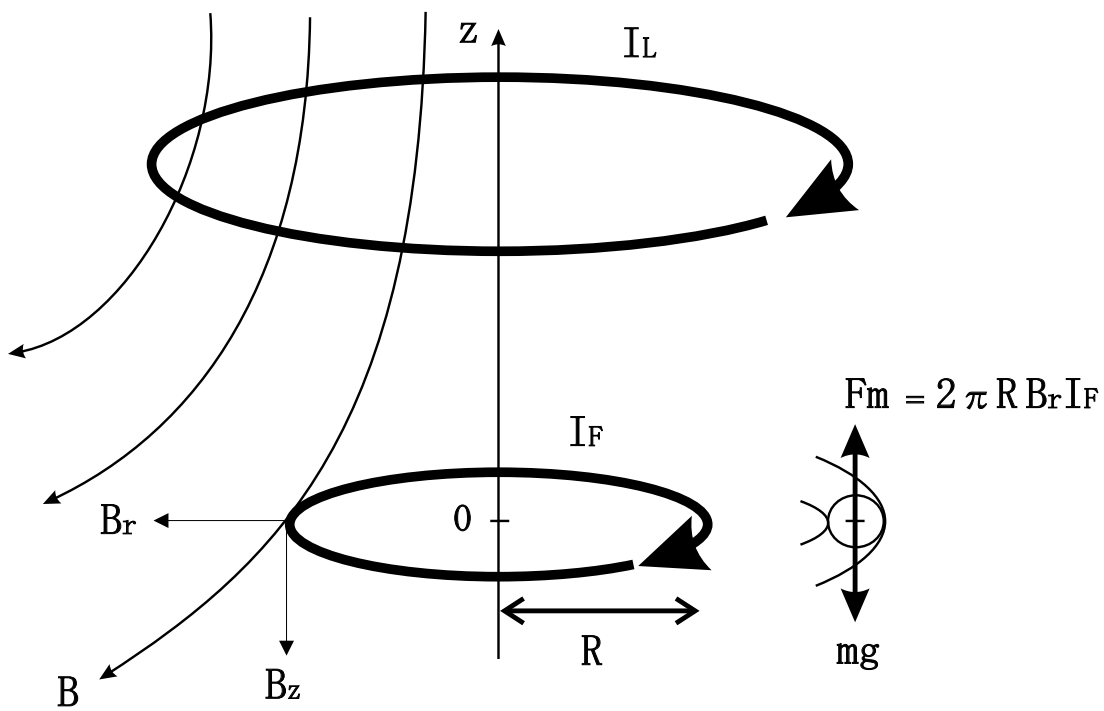


Figure 3.1: The sketch of the model of force balance to the z direction.

3.2 Linear analysis

In the linear analysis we use only eq.3.1. This analysis approximate I_F as a constant.

α is a growth rate of motion and it's expressed as

$$\begin{aligned}\alpha(z) &= \frac{dF_m(z)}{dz} \bigg/ F_m(z) = \frac{d(2\pi R \cdot I_F(z) \cdot B_r(z))}{dz} \bigg/ (2\pi R \cdot I_F(z) \cdot B_r(z)) \\ &= \frac{dB_r(z)}{dz} \bigg/ B_r(z)\end{aligned}\quad (3.3)$$

where F_m is a magnetic force the F-coil feels to the z direction.

A calculation result is shown in Fig.3.2. In the calculation, R is $0.25m$ for a major radius of F-coil, R_L is $0.4m$ for major radius of L-coil and a shape of F-coil is approximated by 9 points.

From the result, there're no stable area in RT-1 device and $\alpha = 4.05$ at $z = 0$ where is the usual levitation region.

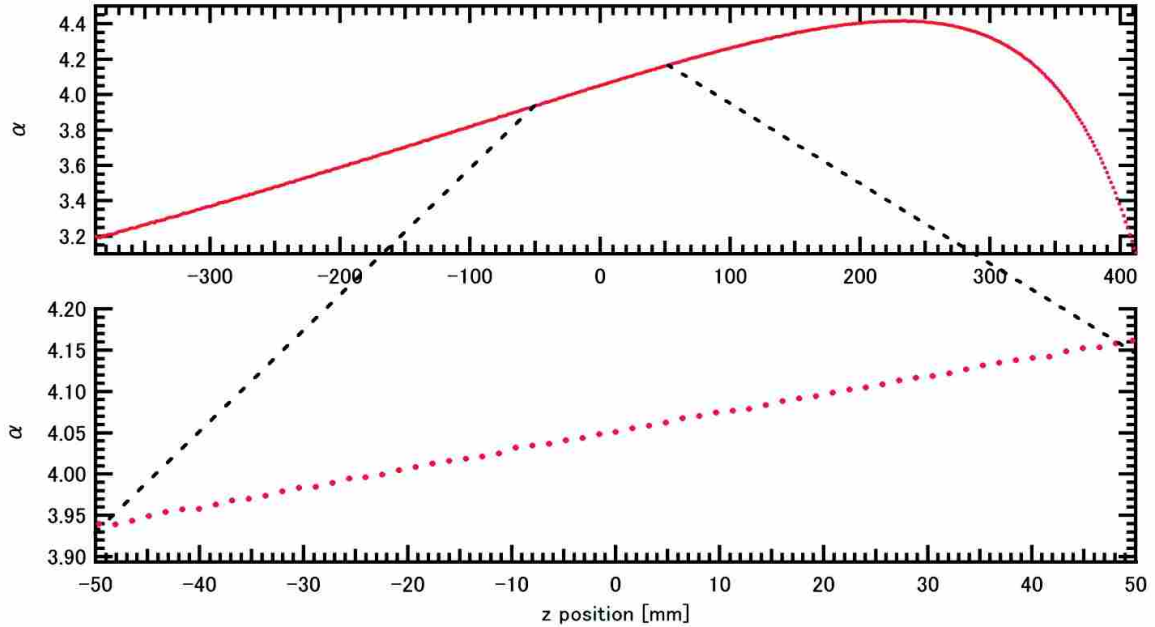


Figure 3.2: z -dependence of z -axis instability by linear analysis

3.3 Nonlinear analysis

The flux conservation is a special feature of superconductor and it always plays a stable role to the z-axis instability. In this analysis, we must note that I_F varies with z position and I_L . We start with defining α as

$$\alpha(z) = \frac{dF_m(z)}{dz} \bigg/ F_m(z) = \frac{d(I_F \cdot B_r)}{dz} \bigg/ (I_F \cdot B_r) \quad (3.4)$$

$$\frac{d(I_F \cdot B_r)}{dz} = B_r \cdot \frac{dI_F}{dz} + I_F \cdot \frac{dB_r}{dz} \quad (3.5)$$

Eq.3.2 means F-coil flux is conserved at any time, and it also means that F-coil flux is conserved at any z position. So from eq.3.2, we derive

$$\frac{d}{dz}(L_F \cdot I_F + M \cdot I_L) = 0$$

Apprximating I_L is constant,

$$\begin{aligned} L_F \frac{d}{dz} I_F + M \frac{d}{dz} I_L &= 0 \\ \frac{d}{dz} I_F &= -\frac{I_L}{L_F} \cdot \frac{d}{dz} M \end{aligned} \quad (3.6)$$

With eq.3.5 and eq.3.6, eq.3.4 becomes

$$\alpha(z) = -\frac{I_L}{I_F L_F} \cdot \frac{d}{dz} M + \frac{dB_r}{dz} \bigg/ B_r \quad (3.7)$$

The second term of eq.3.7 is the α derived in the linear analysis and the first term is an effect of flux conservation. To evaluate this term we need to know a z differential of mutual inductance M and an equilibrium value of I_F and I_L .

3.3.1 Mutual inductance between F-coil and L-coil

Mutual inductance between F-coil and L-coil can be calculated by Neumann's formula approximately. And the z dependence of mutual inductance is derived. Calculation results is shown in figure.3.3. Here F-coil radius is 0.25m and L-coil radius is 0.4m, F-coil wire is 2160 turns and L-coil wire is 68 turns.

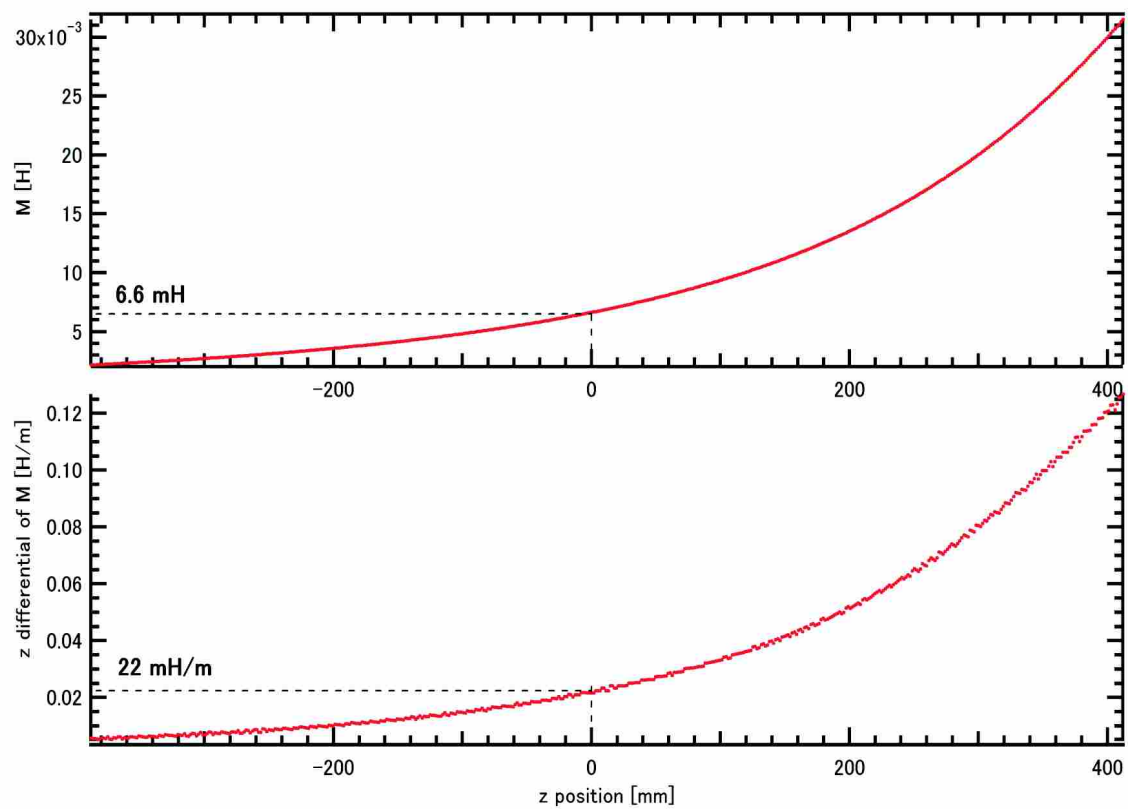


Figure 3.3: Calculation results of z -dependence (upper) and z -differential (lower) of mutual inductance

3.3.2 *z* dependence of I_F and I_L

Next we derive *z* dependence of I_F and I_L at the steady state. When the F-coil is at the steady state, F-coil feels that magnetic force and gravity force are balanced. So

$$2\pi R \cdot I_F \cdot B_r(z, I_L) - mg = 0 \quad (3.8)$$

B_r is a radial magnetic field at the F-coil position and it depends on *z* position of F-coil and I_L .

And the flux conservation also exists

$$\begin{aligned} L_F I_F + M I_L &= L_F I_{F0} \\ I_F &= I_{F0} - \frac{M}{L_F} I_L \end{aligned} \quad (3.9)$$

I_{F0} is the initial F-coil current when $I_L = 0$.

$B_r(z, I_L)$ is proportional to I_L at the same *z* position and, using typical L-coil current value, it can be linearized like

$$\begin{aligned} B_r(z, I_L) &= B_r(z, I_{L0}) \frac{I_L}{I_{L0}} \\ &= B_{r0}(z) \frac{I_L}{I_{L0}} \end{aligned} \quad (3.10)$$

where I_{L0} is typical L-coil current value, if it's not zero anything value is OK.

Substituting eq.3.9 and eq.3.10 to eq.3.8 a quadratic equation of I_L is obtained.

$$\frac{M}{L_F} I_L^2 - I_{F0} I_L + \frac{mg I_{L0}}{2\pi R B_{r0}} \quad (3.11)$$

Because eq.3.11 is a quadratic equation of I_L , if a discriminant is positive there're two real solutions of I_L . The two real solutions is expressed as

$$\begin{aligned} I_L &= \frac{I_{F0} \pm \sqrt{I_{F0}^2 - \frac{M}{L_F} \frac{mg}{\pi R B_{r0}} I_{L0}}}{2 \frac{M}{L_F}} \\ &= \frac{I_{F0} \pm \sqrt{A}}{2 \frac{M}{L_F}} \end{aligned} \quad (3.12)$$

$$\left(A = I_{F0}^2 - \frac{M}{L_F} \frac{mg}{\pi R B_{r0}} I_{L0} \right)$$

We name the solution derived from choosing (+) sign as I_{L+} and the solution derived from choosing (-) sign as I_{L-} respectively.

Then from eq.3.9 and eq.3.12 we can also obtain I_L value. I_L also has two real solutions like

$$\begin{aligned} I_F &= I_{F0} - \frac{M}{L_F} \cdot \frac{I_{F0} \pm \sqrt{A}}{2 \frac{M}{L_F}} \\ &= \frac{I_{F0} \mp \sqrt{A}}{2} \end{aligned} \quad (3.13)$$

We name the solution derived from choosing (+) sign as I_{F+} and the solution derived from choosing (-) sign as I_{F-} respectively. The calculation results of $IL\pm$ and $IF\pm$ are shown in figure.3.4 and figure.3.5. Figure.3.4 is a pair of I_{L+} and I_{F+} which are derived by choosing (+) sign and figure.3.5 is a pair of I_{L-} and I_{F-} which are derived by choosing (-). In the calculation, the initial F-coil current I_{F0} is 115.5A and the mass of F-coil m is 112kg and the inductance of F-coil L_F is 3.3H. And the mutual inductance between F-coil and L-coil comes from figure.3.3. And a shape of F-coil and L-coil is approximated by 9 points respectively in B_r calculation.

3.3.3 z-axis instability in the nonlinear analysis

α in the nonlinear analysis was expressed eq.3.7. From 3.3.1 and 3.3.2 we obtained z dependence of z differential of mutual inductance M and z dependence of an equilibrium value of I_F and I_L . Finally we can evaluate α in the nonlinear instability eq.3.7.

Because a pair of I_L and I_F has two real solutions respectively by choosing (+) or (-) sign in the quadratic equation, α also has two real solutions such as α_+ and α_- . Results of the calculation is shown in figure.3.6.

3.4 Consideration

z-axis instability is derived in the case of the RT-1 F-coil. There're two types of levitation, one needs 430A L-coil current and other needs more than 1MA. The former type is unstable to z-zxis, $\alpha = 4.05$ at $z = 0\text{mm}$, and the latter type is stable to z-axis, $\alpha = 13500$ at $z = 0\text{mm}$. This means that the latter type is "self-stable" as a consequence of flux conservation, but this type of levitation needs too much L-coil current to realize in the RT-1 device.

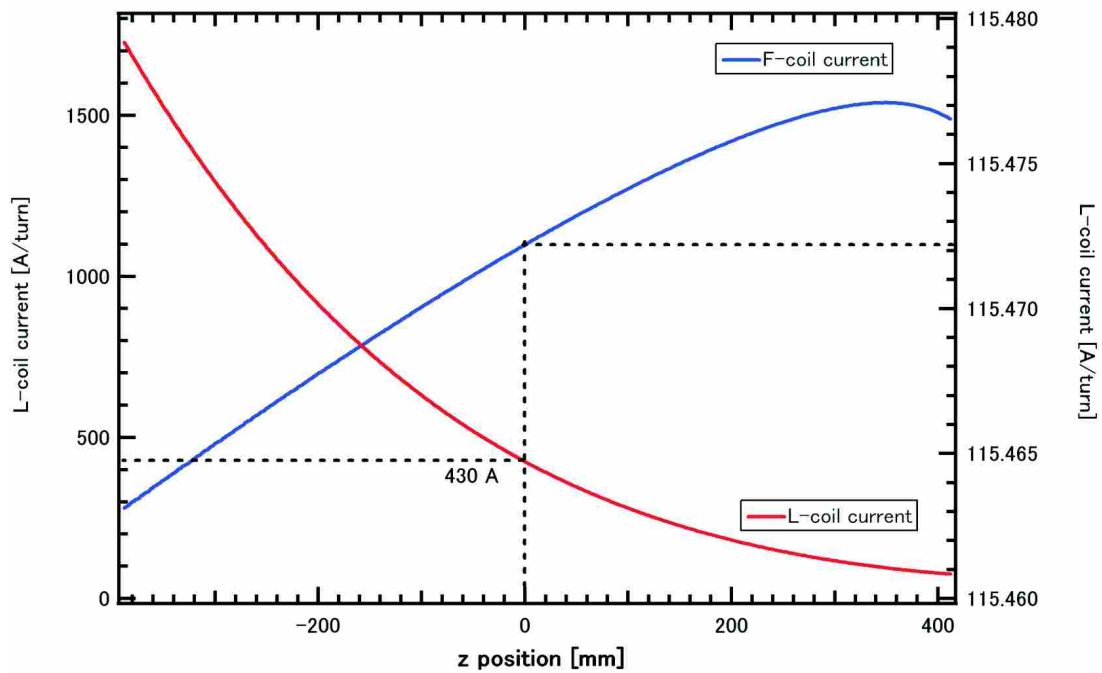


Figure 3.4: Calculation results of z dependence of I_{L+} (red line) and I_{F+} (blue line)

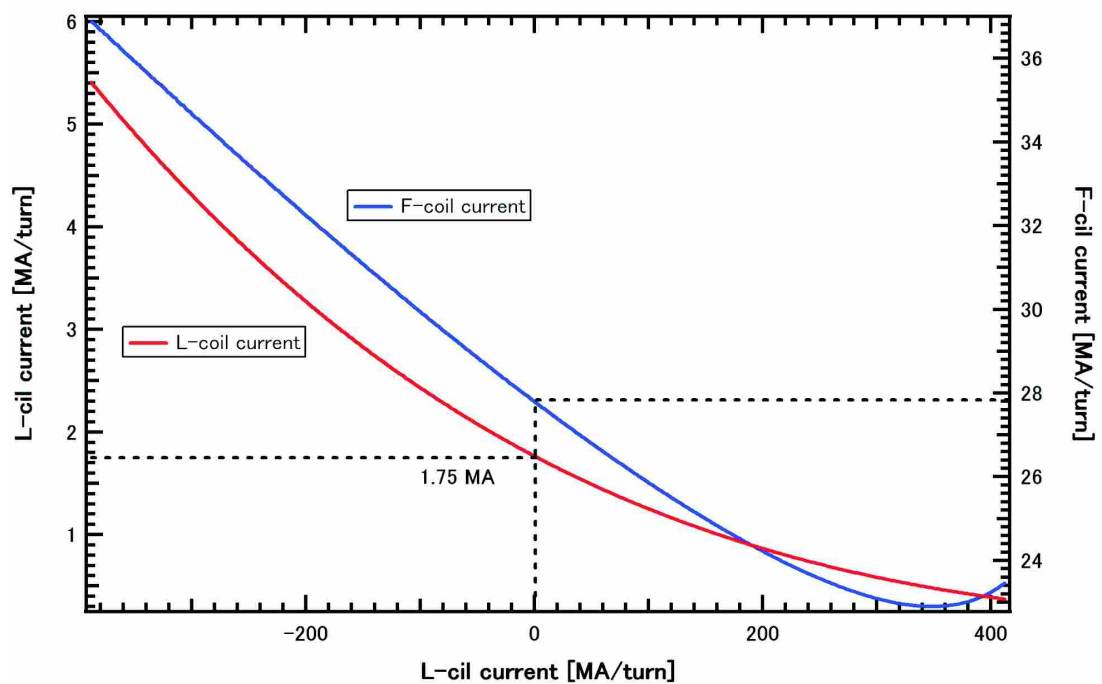


Figure 3.5: Calculation results of z dependence of I_{L-} (red line) and I_{F-} (blue line)

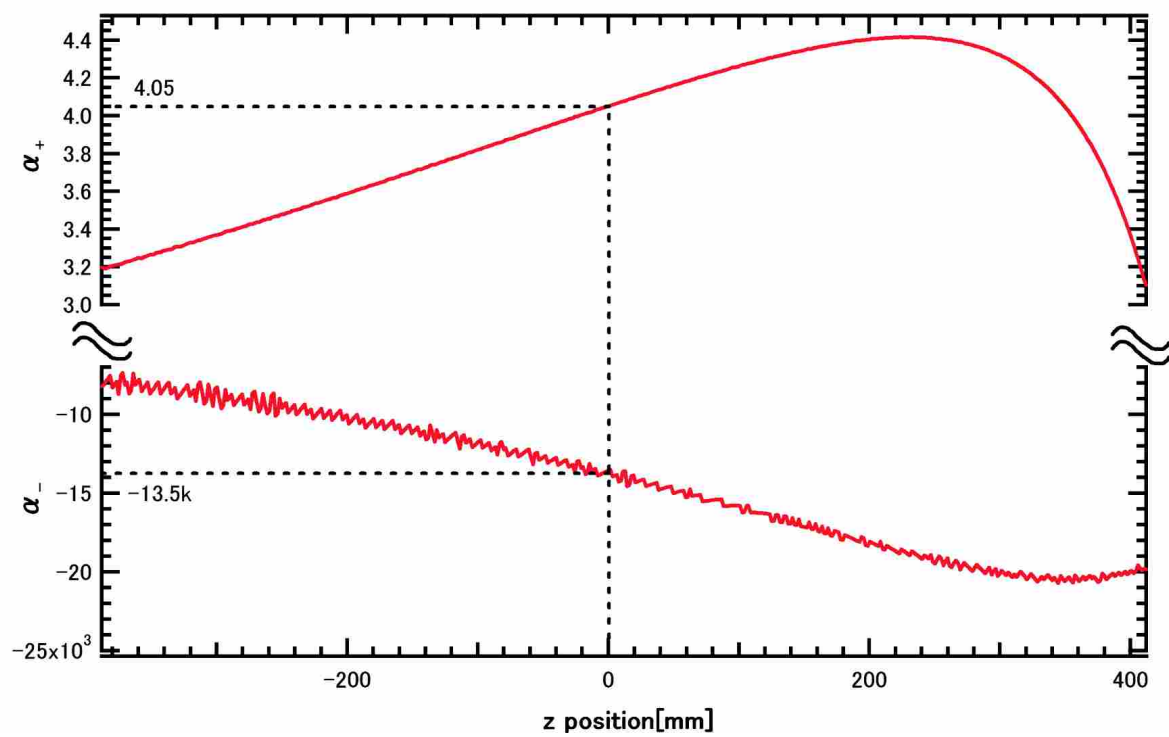


Figure 3.6: Calculation results of z dependence of α_+ (upper) and α_- (lower)